Structural Processes at Slow-Spreading Ridges

John C. Mutter and Jeffrey A. Karson

Slow-spreading (<35 millimeters per year) mid-ocean ridges are dominated by segmented, asymmetric, rifted depressions like continental rifts. Fast-spreading ridges display symmetric, elevated volcanic edifices that vary in shape and size along axis. Deep earthquakes, major normal faults, and exposures of lower crustal rocks are common only along slow-spreading ridges. These contrasting features suggest that mechanical deformation is far more important in crustal formation at slow-spreading ridges than at fast-spreading ridges. New seismic images suggest that the nature and scale of segmentation of slow-spreading ridges is integral to the deformational process and not to magmatic processes that may control segmentation on fast-spreading ridges.

Seafloor spreading involves the closely linked processes of magmatism and mechanical extension. The relative importance of each of these processes in accommodating lithospheric strain and in controlling the principal observable manifestations of plate separation is strongly dependent on spreading rate. At spreading centers where the half-rates are greater than about 50 mm/yr several lines of evidence suggest that magmatism is the dominant process: the axial morphology is characterized by an elevated volcanic edifice that in many cases includes a small, shallow fault-bounded depression at its summit that may be the expression of caldera collapse [Fig. 1A (*1–3*)]; there are abundant recent eruptions and lava flows (*1, 2, 4*); magma bodies in the upper crust have been imaged for tens of kilometers along several fast-spreading ridges (*5–7*); and earthquake activity indicative of mechanical deformation of the crust is low (*8*). In contrast, at slow-spreading ridges mechanical extension plays a critical role. The axial morphology is almost the inverse of that at fast-spreading ridges. Slow ridges are defined by a distinct, broad depression (Fig. 1B)—a structure so diagnostic of slow seafloor spreading that it was recognized in the earliest studies of the global mid-ocean ridge system (*9*). The thermal structure of the axial region (*10*) and the discontinuous nature of recent eruption centers (*11*) virtually preclude the presence of extensive, long-lived magma bodies, and none have been detected by seismic methods (*12, 13*). Near-bottom observations have documented surface faulting throughout the axial depression (*14*); the fault scarps create a stairstep morphology to the valley walls and an overall geometry that strongly recalls that of continental rift valleys (Fig. 1C). Earthquake activity is nearly continuous (*8*) and source mechanisms indicate that normal faulting commonly extends through the crust and into the upper mantle. The total earthquake moment release implies that at least 20% of total plate separation is accommodated by mechanical extension.

Both slow-spreading and fast-spreading ridges are morphologically segmented. The axial depths and cross-sectional profiles of the ridges vary systematically along strike with a wavelength of 20 to 50 km. A segment usually comprises the region centered on an along-axis high between two along-axis depressions. Study of the morphologic variations, geophysical signature, and geological patterns, primarily within and between fast-spreading segments (*15–17*), has led to the conjecture that segmentation of fast-spreading and slow-spreading ridges owes its origin to discrete zones of mantle upwelling (*18*). Despite the evidence that deformational processes have a major influence on slow-spreading ridges, mechanical processes have generally been considered secondary to segmentation.

In this article we relate the surface observations on slow-spreading ridges to the complex fabric of reflectivity internal to the oceanic crust revealed in new seismic imaging (*19–24*). This pattern records the response of the whole crust to tectonic and magmatic processes. These coupled observations allow us to develop a mechanical model of crustal accretion at slow-spreading ridges in which segmentation is an integral part.

External Expression of Slow Spreading

The axial depression of slow-spreading ridges is typically more than 1 km deep and as much as 40 km wide [Fig. 2, A and C (*14, 25, 26*)]. The depression is at least partly the result of brittle failure of the crust by mechanical extension; multibeam bathymetric mapping has revealed the presence of numerous steep, linear slopes of fault scarps (Fig. 2, A and B). High-resolution side-scan sonar images also contain highly reflective linear features that represent fault scarps modified by mass wasting (*14*). Submersible observations and deep-towed camera studies have shown that fissuring and small-offset, high-angle faults are active throughout the axial depression and its inner walls (*27–29*). Teleseismic earthquake and microseismicity (*30–32*) studies show that some normal faults rupture to depths of as much as 8 to 10 km, at least the full thickness of the crust. The concentration of most earthquakes below the walls of the axial valley of the Mid-Atlantic Ridge (MAR) suggests that these are the sites of the deepest faulting (*33*). A detailed microseismicity study (*30*) of the MAR near 23°N has shown that a single planar normal fault extending to a depth of 8 km bounds the eastern rift valley and defines a relatively simple half-graben.

Plutonic mafic and ultramafic rocks are exposed in wide areas in ridge-parallel escarpments along the median valley walls of many slow-spreading ridges and in transform zones [Fig. 2A (*34–38*)]. Similar rocks

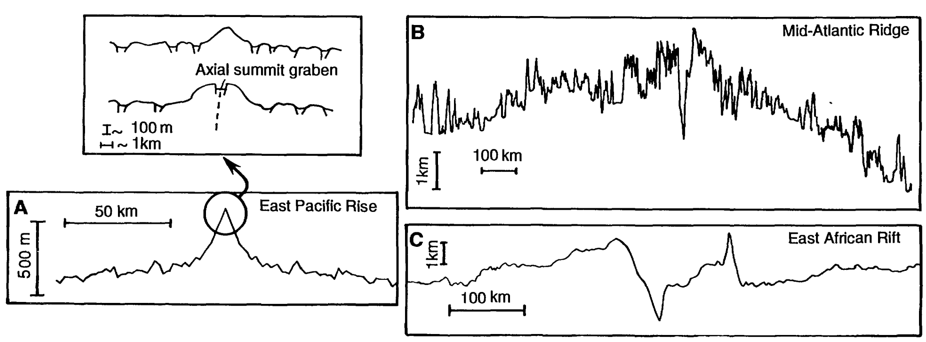

Fig. 1. Comparison of morphologic profiles of the East Pacific Rise (*3*) (**A** and inset), the Mid-Atlantic Ridge near the equator (**B**), and the East African Rift at Lake Tanganyka (**C**). The latter was used more than 30 years ago by Heezen (*9*) to draw attention to the basic similarity between the continental rifts in East Africa and the morphology of slow-spreading ridges. Note the different scales.

J. C. Mutter is at the Lamont-Doherty Geological Observatory and Department of Geological Sciences, Columbia University, Palisades, NY 10964. J. A. Karson is in the Department of Geology, Duke University, Durham, NC 27706.

have been recovered from shallow drill holes and dredges in old crust formed at slow-spreading ridges (39, 40). These rocks are commonly regarded as a major component of fast-spreading crust but are not known to be exposed at fast-spreading ridges. Constraints from fluid inclusions in recovered oceanic metagabbros (41), the distribution of these rock types in ophiolites (42, 43), velocity data from seismic refraction studies (44), and deep drilling in the oceanic crust (45) all suggest that the mafic and ultramafic rocks must have been exhumed from the middle and lower crust and upper mantle at depths of 2 to 6 km beneath the seafloor. Exposure from these depths cannot be accomplished by closely spaced, high-angle normal faulting. Movement on low-angle normal (detachment) faults can, however, unroof deep structural levels. A major low-angle (~30°) normal fault has been observed cutting gabbroic rocks and serpentinites in the MARK area of the MAR [Fig. 2 (38, 46, 47)], where the median valley intersects the Kane transform fault. The western flank of the rift valley rises to depths as shallow as 1000 m and forms an elevated structure termed an inside corner high (Fig. 2A), typical of those found where slow-spreading ridges intersect large-offset transform faults. The entire western axial valley wall here is essentially a single normal fault surface dipping 30° to the east. Gabbros, metagabbros, and serpentinites are exposed along the fault surface. The rocks contain foliations, shear zones, and discrete fault surfaces that generally parallel the surface slope. The relief across this inside corner high is at least 3.5 km, part of which must have been produced by flexural uplift of the unloaded footwall block. Similar rocks are exposed for nearly 40 km to the south of the ridge-transform intersection. Low-angle detachment faulting has also been proposed as the mechanism for exposing the metagabbros drilled [Ocean Drilling Program (ODP) Leg 118] near the Atlantis II fracture zone on the Southwest Indian Ridge (48) and has been

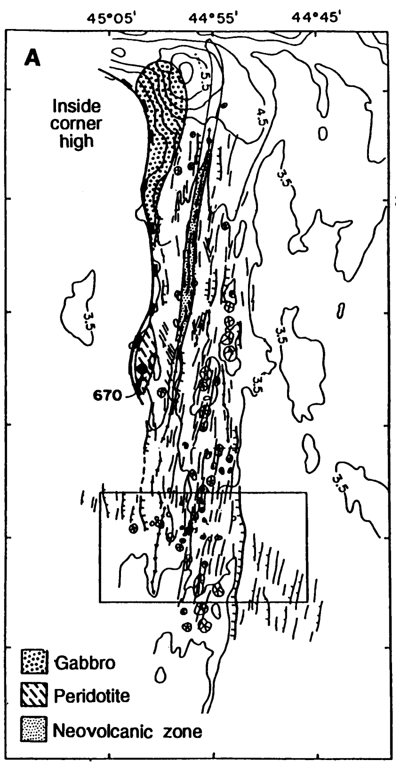

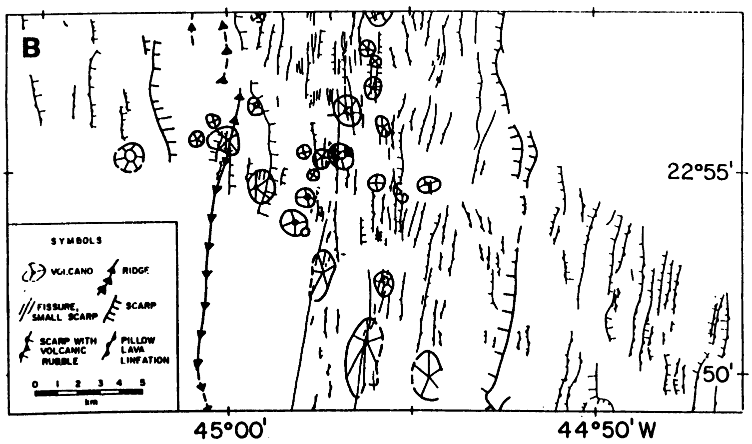

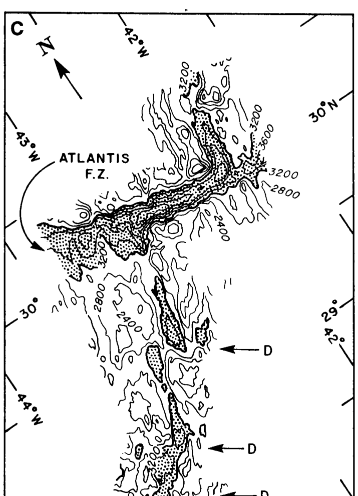

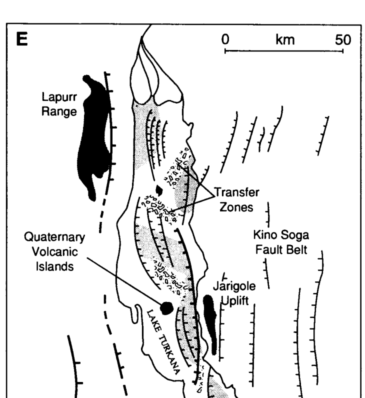

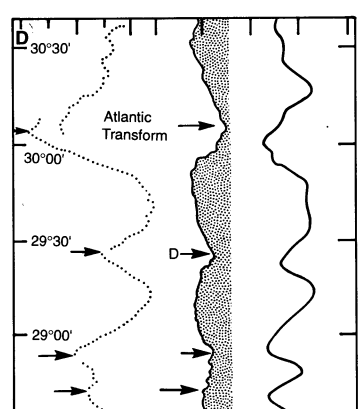

Fig. 2. Surface geologic structure in the MARK area of the MAR (**A** and **B**) compiled from the results of bathymetric mapping and side-scan sonar imaging (*14*) and submersible observations (*11, 29, 35, 38*). Exposures of the lower crust and upper mantle occur extensively on the western flank of the axial valley. The number 670 refers to an ODP drill site where serpentinized peridotite was recovered (*39, 40*). (**C**) The bathymetry of the MAR (*25*). The axial depression, shown by the stippled area (depths > 3200 m), varies in width along strike and is offset at locations described as ridge axis discontinuities, noted with a "D." (**D**) Along-axis profile of the bathymetry (center profile) and Mantle Bouguer (M.B.) anomaly (left profile), and the variation in depth to Moho (right profile) inferred from the gravity pattern (*55*). Discontinuities shown with arrows correspond to those in (C). (**E**) Basic structural elements of Lake Turkana in East Africa [in part after (*83*)]. Depocenters are shown in gray shading, accommodation (transfer) zones are shown with coarse, pebbly symbol, and volcanic centers as heavy shading.

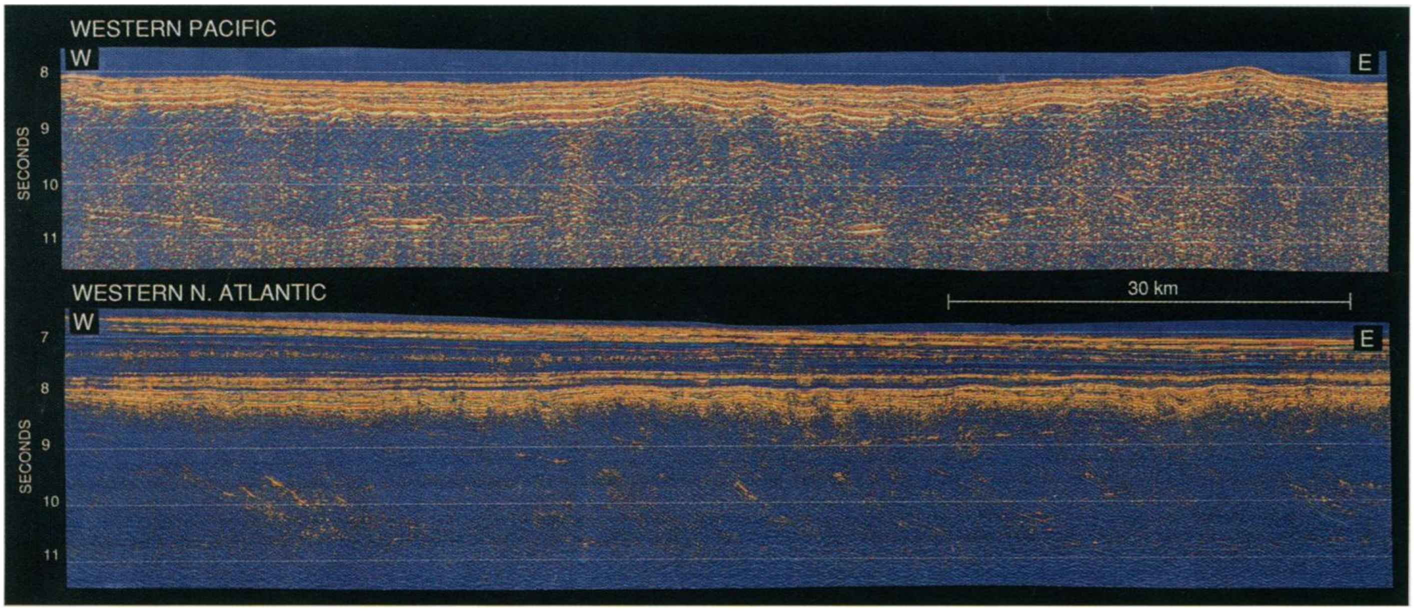

Fig. 3. Comparison of seismic images (*19*) of oceanic crust produced at fast spreading rates in the western Pacific off Japan (**top**) with crust produced at slow spreading rates in the western North Atlantic (**bottom**). Crustal age is approximately 140 million years ago in both cases, but the spreading rate differs by almost an order of magnitude. Sediments, represented by the roughly horizontal stratified sequences, are thicker in the Atlantic profiles—the top of the crust lies at about 8.5 s in the Pacific and about 8.2 s in the Atlantic data. Reflection Moho is a strong reflection in the western Pacific data at about 10.5 s and is a much less distinct reflection in the western North Atlantic data at about 10.75 s.

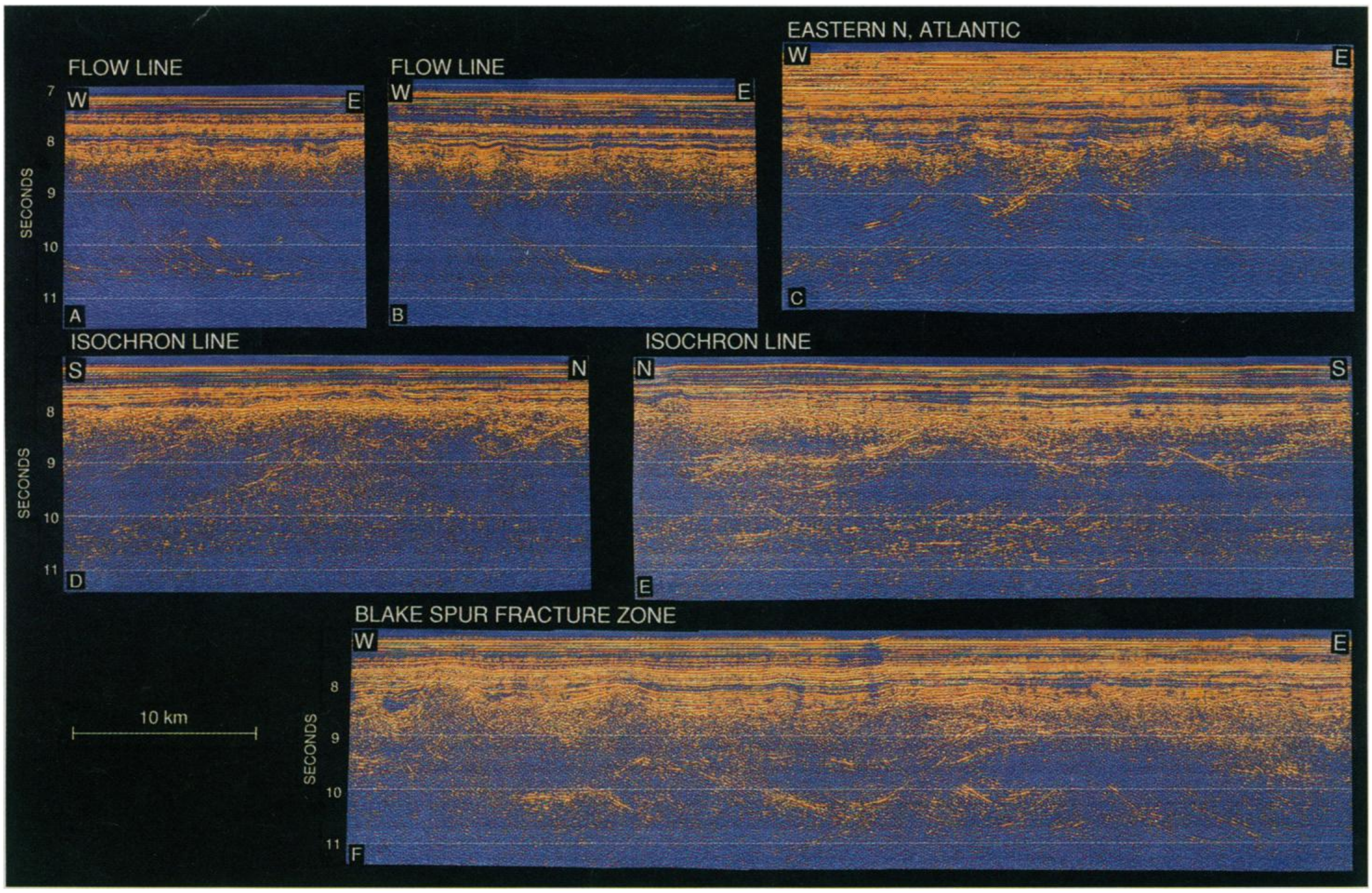

Fig. 4. Seismic images (*19*) of oceanic crust produced at slow spreading rates in the North Atlantic illustrating a variety of forms of reflectivity described in detail in the text. Image (**C**) is from the eastern North Atlantic (*24*); the others are from the western North Atlantic. The sediment-basement interface occurs at about 6 s in (C) and at a little over 8 s in the other profiles. (**A**) and (**B**) are from flow-line profiles, (**D**) and (**E**) are isochron lines, (C) is oblique to the spreading direction, and (**F**) is from the trough of the small-offset (about 12 km) Blake Spur fracture zone.

recognized as an important process in a number of ophiolites thought to have been produced at slow-spreading ridges (*49–52*).

Morphologic segmentation of slow-spreading ridges occurs on a scale of 20 to 50 km through variations in the axial depth, from highs at the segment centers to lows at the boundaries (Fig. 2, C and D). These are accompanied by changes in the relief, width, and structural style of the axial depression. The axial depression has its lowest relief and is typically poorly defined at the segment centers, where the floor of the depression has risen to depths close to that of the ridge flanks. The greatest relief (as much as 6 km; more than twice the normal relief) and asymmetry is normally developed where the axis intersects a major transform as, for instance in the MARK area (Fig. 2A). Here the inner rift flank shoals markedly to form the inside corner high, whereas the outer rift flank and axial depression are deep. Similar structures with smaller relief are common at minor ridge offsets. Intrusion of magmas creates elongate edifices (neovolcanic ridges) or clusters of volcanoes in the deepest parts of both symmetrical and asymmetrical depressions and shows no apparent preferred location within either (Fig. 2, A and B). The along-axis highs that occur at segment centers typically lack neovolcanic ridges. Axial depressions are laterally displaced and overlap slightly at some segment boundaries (such as at 29°23′N on the MAR, Fig. 2C). Elevated structures that may be even shallower than the highs associated with the centers of segments are present between many overlapping depressions. Less prominent highs are present at segment boundaries where the axial depressions are offset but do not overlap (such as at 28°50′, Fig. 2C). Segments boundaries appear to have migrated along the ridge, creating V-shaped wakes (*53*).

The segmented nature of seafloor accretion at slow-spreading ridges is also expressed in the gravity signature (Fig. 2D). Both the North and the South Atlantic Ocean basins show a strong inverse correlation of bathymetry to the residual mantle bouguer anomaly (*54, 55*); gravity lows are generally centered over the along-axis highs at the centers of the segments. If the origin of the anomalies is attributed entirely to variations in crustal thickness, along-axis thickness changes of up to 3 km are implied, even for regions well away from major transform faults (Fig. 2E). Earthquakes and earthquake swarms also appear to be related to the basic segmentation: Most are preferentially located in or near the depressions of major half-grabens (*33*).

Continental rifts are also known to be segmented (*56–64*) into half-grabens and full grabens that vary in length from 40 to 120 km and are linked end-to-end by transfer (or accommodation) zones that are typically elevated (Fig. 2E). Transfer zones are areas of distributed crustal strain that permit adjacent rift segments to extend with different geometries and at different rates. In areas of substantial crustal magmatic construction, such as the eastern branch of the East African Rift or the Main Ethiopian Rift, volcanic centers and elongate ridges tend to lie near the centers of the half-graben rift segments (*63*) and are less commonly associated with accommodation zones. This type of structural segmentation, originally identified in the African rift system (*57*) and now known to occur widely in diverse regions of extension including back-arc basins (*64*), is clearly the response to extensional processes and does not require magmatic processes for its formation.

Internal Expression of Slow Spreading

The morphology of mid-ocean ridge spreading centers, particularly slow-spreading ridges, is typically rough, and seismic images of them are distorted and unclear (*13*). Oceanic crust is transported away from the ridges by continued spreading where it becomes the floor of deep ocean basins and is typically covered with several hundred meters of sediments, which bury the rough topography. Seismic images from these old basins provide clear images of the internal structure of the oceanic crust (Figs. 3, 4, and 5). In the western Pacific (*65*), the crust has been created at rates greater than 60 mm/yr and is essentially transparent to seismic energy (Fig. 3, top). A strong, quasi-continuous reflection often appears at about a 2-s reflection time beneath the basement (corresponding to a depth of about 6 km) and is usually referred to as the reflection Moho (*65, 66*). Reflections have been recognized beneath the Moho near the ridge axis (*67, 68*) but have not been described in older crust.

Crust created at slower rates, such as the Cretaceous-aged crust in the North Atlantic (half-rate of 15 mm/yr) exhibits a rich variety of reflecting horizons [(*21–24*) Figs. 3, bottom, 4, and 5]. Typically the shallow crust contains distinct, subhorizontal reflec-

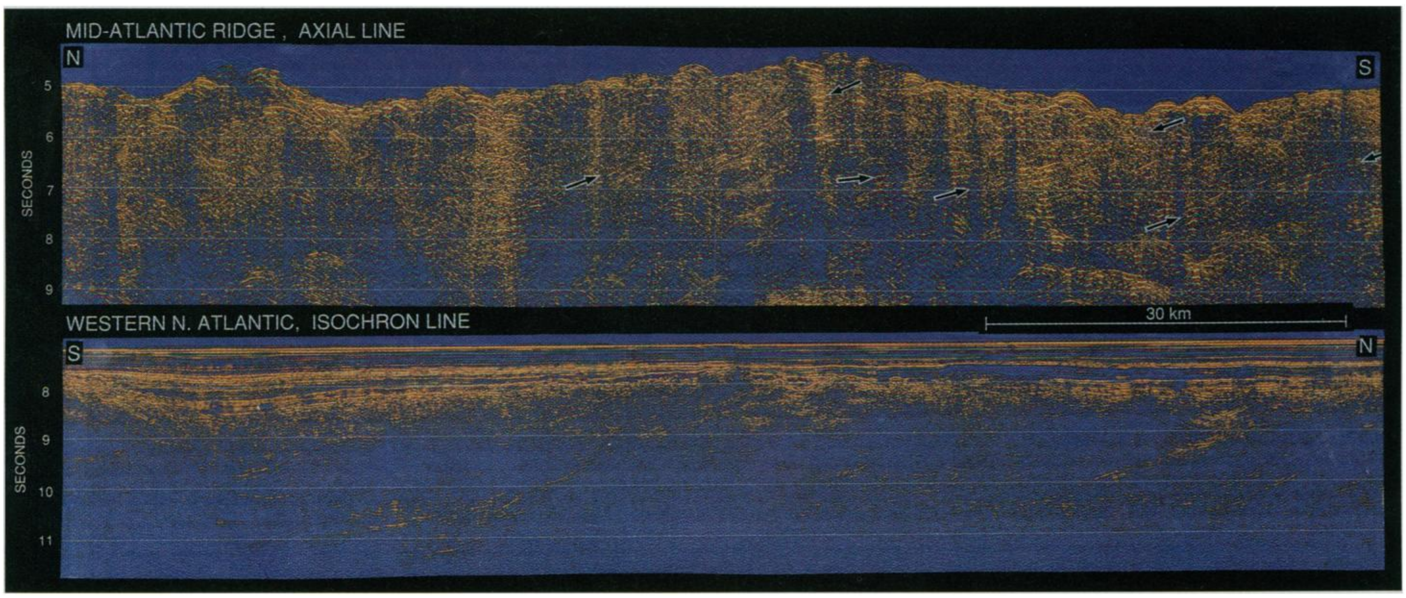

Fig. 5. Comparison of seismic images (*19*) of crust from an isochron-line profile in the western North Atlantic (**bottom**) with an image obtained along the axial depression of the MAR (**top**) in the MARK area (Fig. 2A). Image quality is poorer in the MARK profile because no sediments have accumulated on the seafloor and the hard, rough surface scatters energy throughout the section. Arrows identify significant reflections.

tors and the middle crust is almost transparent. The lower crust exhibits the strongest and most diverse reflectivity comprising a diffuse background together with distinct banded patterns of strong, linear, or arcuate dipping reflectors with highly variable spacing. There is seldom a distinct Moho reflection in crust produced at slow spreading rates; the reflective lower crust typically gives way to a transparent mantle beneath. Where the lower crust is poorly reflective its base can be difficult to recognize. Similar patterns of reflectivity have been reported elsewhere where crust was created at slow spreading rates: Cuvier Basin off northwest Australia (*69*), Panama Basin (*45, 70, 71*), and the eastern Gulf of Guinea (*72*). These observations suggest that crust acquires significant internal reflectivity at the same spreading rate at which the axial region of spreading centers develops a distinct median valley and, hence, the rate at which plate separation is accompanied by significant mechanical extension.

The diffuse low-amplitude reflectivity in the lower crust is pervasive throughout seismic images from the eastern North Atlantic. This reflectivity pattern terminates at a near-constant total reflection time of 10 to 11 s which, from refraction seismic data in the region (*73*), corresponds to Moho. The upward boundary is variable, and this gives rise to an undulating appearance of the onset of diffuse reflectivity. In some places, this diffuse reflectivity extends into the shallowest crust and even reaches the sediment-basement interface. There is only a weakly developed, subhorizontal fabric; the typical appearance is of a chaotic sequence of short reflectors (the speckled, yellow cloud, lower part of Figs. 3B and 4).

The strong reflectors in the lower crust (Figs. 3, bottom, and 4) occur with almost equal average spacing on flow (*74*) lines (5.5 reflectors per 100 km) and on isochron (*74*) lines (6.0 reflectors per 100 km) in the western North Atlantic (*23*). The spacing on flow lines corresponds to a reflector being formed about once every 1.2 million years. They dip at approximately 30° toward the spreading axis on flow lines and approximately 20° to the south on isochron lines. Most of the strong reflectors are confined to the same depth interval as the diffuse reflectivity. In the North Atlantic near the Canary Islands (*24*) (Fig. 4C), the crust shows similar patterns of reflectivity. The basement locally consists of large tilted blocks, and the strong reflectors have an arcuate shape that coincides with the downward projection of the westward facing flank of the block.

Although most of the dipping reflectors are in the lower crust, an important subset is much longer and can be mapped from the lower crust into the middle and upper crust and locally to the top of the crust. Many of these elongate reflectors have a sigmoidal shape (Figs. 4 and 5). Elongate reflectors are much more commonly observed on isochron lines, and their dip is generally shallower than those seen on flow lines (*23*). The strength and complexity of the elongate reflectors increase down-dip from a single, sharp horizon in the middle crust that broadens into a package of several stronger reflectors in the lower crust. The broadening and increase in strength occur with the onset of the diffuse lower crustal reflectivity. In many instances, particularly where they traverse the whole crust, strong dipping reflectors demark roughly triangular-shaped zones of diffuse reflectivity (Figs. 4, E and F, and 5, lower panel). When seen in this relation, the diffuse reflectivity locally shows a preferred fabric that is orthogonal to the dip of the strong reflector that forms the boundary.

One of the most spectacular examples of structure that appears to disrupt the whole crust was imaged along the trace of the Blake Spur fracture zone (Fig. 4F). Here a single surface can be recognized that is near horizontal in the upper crust and bifurcates into two structures that dip through the middle crust and then flatten again at different levels in the lower crust. Refraction seismic studies (*73*) suggest that the deeper of these reflectors penetrates into the mantle, which lies at a reflection time of about 10 s. The Blake Spur fracture zone offsets magnetic lineations by only about 12 km (*73*), comparable to the offset of some ridge discontinuities south of the Atlantis fracture zone (Fig. 2C) but much smaller than the offset of the fracture zone.

The North Atlantic seismic images (Figs. 3 and 4) describe structure in mature crust located some considerable distance from spreading centers. It could therefore be argued that the crust may have acquired these structures as part of an aging process, and hence it is important to examine images from the axial region of an active spreading system to establish if similar structures are present there, even though image quality from these regions is typically low. A profile from the axial depression of the Mid-Atlantic Ridge in the MARK area (*13*) (Fig. 5, top) includes two along-axis highs and associated depressions like those described by Lin *et al.* (*55*) (Fig. 2, C and D). No reflection Moho can be recognized, but several indistinct, northward-dipping reflectors (indicated by arrows) are just evident above the background noise. These reflectors trend toward the surface near the along-axis depressions. We compared this profile with a much higher quality image

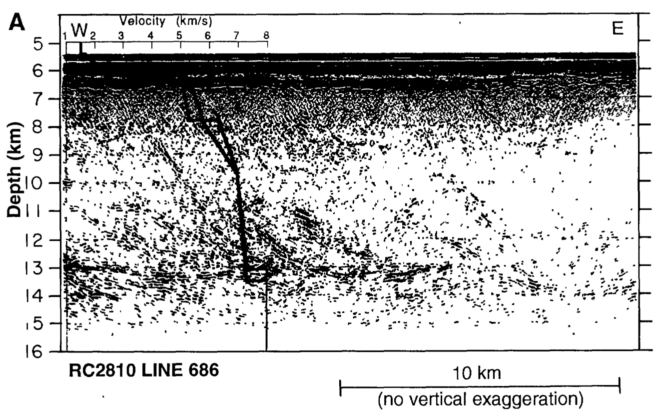

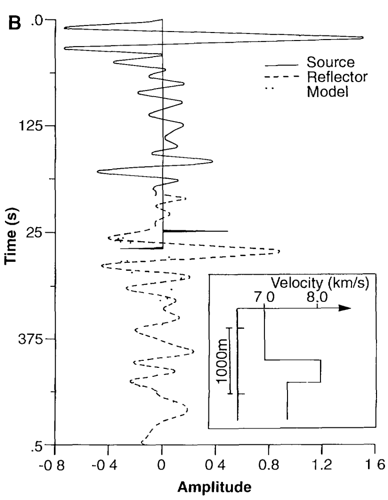

Fig. 6. Characteristics of the strong dipping reflectors. (**A**) is a comparison of velocity-depth profiles obtained from seismic refraction experiments in the western North Atlantic area (*73*) with the seismic reflection image obtained at the coincident location. The two velocity-depth profiles pertain to different components of the same experiment. Reflection Moho coincides with the increase to velocities greater than 8 km/s, but the onset of lower crustal reflectivity is not associated with a distinct boundary in the velocity-depth profiles. (**B**) shows waveform analysis of the deep strong reflector in Fig. 4B. A scaling of six was applied to the reflected arrival to show its waveform more clearly and to illustrate the match of the calculated waveform to the observed data. The calculated reflection coefficients are shown as spikes, the sizes of which are a direct measure of the reflection coefficient after dividing by the amplitude scaling factor. The calculated reflection coefficient at the top of the layer is 0.123, only about half that of the seafloor. The structure giving rise to the reflection shown in the inset box can be modeled as a simple thin layer having a velocity of 8 km/s, approximately the velocity of mantle rocks.

from the western North Atlantic (Fig. 5, lower panel) that shows several clear reflectors dipping at shallow angles across the whole crust. From this comparison we conclude that major through-going structures are indeed present in the actively spreading MARK area and that their dip, length, and spacing closely match those of structures imaged in the ancient crust.

Two other features of the dipping reflectors give clues to their origin. First, most of the dipping reflectors and associated diffuse reflectivity are in that part of the crust with the most uniform velocity-depth structure determined from seismic refraction studies (73)—seismic layer 3 (Fig. 6A). Second, the waveforms of individual reflectors can be modeled (75) to derive estimates of the layer structures responsible for the reflections. Individual field-recorded traces show that the strong reflectors have waveforms that are remarkably similar to the original source pulse (Fig. 6B). Eight of the strongest lower crustal reflectors have been analyzed. If the reflectors are the response of a single layer, the best estimate of layer thickness is 100 m. The required material velocity in the layer for a background velocity for layer 3 derived from the refraction seismic study (73), is about 8 km/s, which is the velocity of mantle rocks.

Slow Seafloor Spreading Processes

Schematic, perspective block diagrams of several spreading segments of a notional ridge (Fig. 7) and of the details of one portion of the ridge (Fig. 8) portray the first-order structural features of a model that accounts for relations between internal and external expressions of ridge tectonics. We propose that essentially all the external and internal characteristics of the axial region described above can be attributed to deformational processes. Magmatic injection events that build the crust are spaced sufficiently in time at slow-spreading rates that plate separation by mechanical extension is the primary factor controlling the time-integrated structure of the crust and the shape of the slow-spreading center. At any time, the shape of the spreading center will be determined by a combination of volcanic and structural processes.

The internal structure and morphology of the notional ridge's rifted axial depression (Figs. 7 and 8) are controlled by a system of linked fault zones defined by the strong, banded reflectors in the seismic profiles (Figs. 3, 4, and 5). They comprise interconnected normal, oblique-slip, and strike-slip faults. Reflections crossing the entire crust (Figs. 4 and 5) are interpreted to be normal-sense detachment faults that allow for relative displacement of upper and lower crustal sections. These are the subsurface expression of the exposed fault planes that define the walls of the deep asymmetric half-graben that typify segment boundaries (Fig. 2A). The major faults have an asymmetric spoon shape and are elongated parallel to the spreading axis. Because of this shape, both seismic profiles along either isochrons or flow lines may image the same structure (Fig. 8). Flow lines cross structures with relatively high dips (~30°) and contain the inferred slip direction of the detachment; isochron lines cross relatively low-angle (~20°) structures, are closer to the strike of the detachment, and are normal to the inferred slip direction on them. Movement on the system of faults creates large blocks with the three-dimensional geometry of elongate lozenges of crustal and upper mantle material. The lozenges are interlinked, but structurally independent units, each underlain by a single major detachment. The geometry of the detachment surfaces, and hence the size and shape of the elongate lozenge structures (Figs. 4, E and F, and 5), controls the size and shape of the axial depression of slow-spreading ridges. We consider that this process is the underlying mechanism that scales their segmentation length.

Extensional deformation occurs by both brittle and ductile mechanisms. The diffuse reflectivity and associated reflecting bands in the lower crust are considered to represent the expression of ductile deformation. We suggest that the pervasive diffuse sequences represent distributed bulk coaxial extension in the ductile field (pure shear) and that the dipping, banded reflectors represent concentrated deformation in brittle-ductile shear zones. As the region of brittle deformation moves downward into the crust as it cools, brittle structures may merge with or capture concentrated zones of ductile deformation (76). The distinct, roughly triangular-shaped regions of diffuse reflectivity (Figs. 4 and 5) may outline such regions of dilational strain in the footwall blocks of major faults, as recently described for footwall blocks in continental rifts (77). As for the major detachment structures, these triangular zones are observed on both flow lines and isochron lines (Fig. 8). The highly reflective nature of the banded reflectors in the diffuse sequences may be caused by compaction-driven migration of intercumulus melt from a crystallizing magma body into porous ductile shear zones (78). Chemical exchange, precipitation of oxides, and trapping of these melts alter the gabbros in the shear zones to high-density ferrogabbros. The occurrence of such bands in a background of lower density gabbros could provide the elastic property contrast required to produce the strong reflectors.

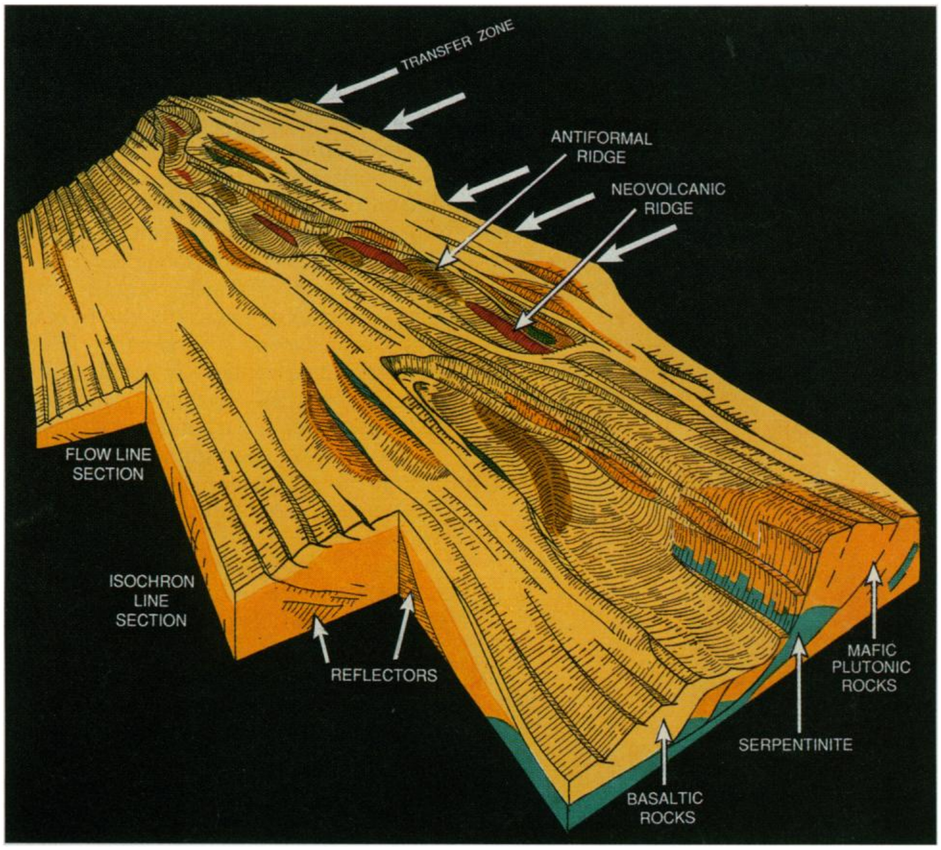

Fig. 7. Schematic perspective model of a notional slow-spreading ridge axis and adjacent flanks. See text for discussion.

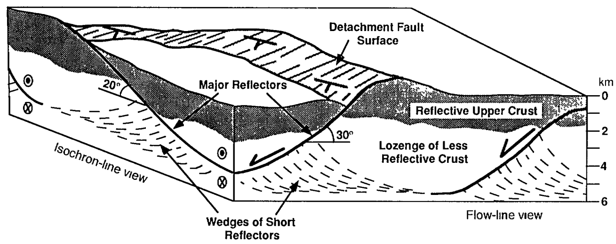

Fig. 8. Block diagram illustrating the relation between major crustal detachment surfaces imaged in flow line and isochron line seismic data (Figs. 3, 4, and 5). The same detachment is imaged on both profiles because it dips obliquely with respect to the spreading direction. Vertical offsets may appear in the isochron line images even though the displacement direction is actually at a high angle to the section.

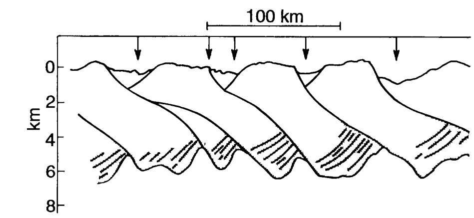

Fig. 9. Crustal thickness variations along the axis of the Mid-Atlantic Ridge in the North Atlantic derived from gravity data (*55*) are reinterpreted to be the result of structural processes that deform the crust, rather than thickness variations associated with plumes of upwelling magma (*55*). The geometry of the fault structures traversing the crust matches those seen in isochron lines imaged by seismic methods in the North Atlantic (Figs. 4 and 5). We have not altered the shape of the Moho from that presented by Lin *et al.* (*55*) in making this illustration.

The front part of the notional ridge (Fig. 7) lies adjacent to a major ridge offset and has evolved by the greatest amount of mechanical extension. Structures here are modeled after images from the trough of the Blake Spur fracture zone (Fig. 4F). We interpret these structures to be a major detachment system. Flat-ramp-flat features define an extensional duplex. This highly extended area is associated with the thinnest crustal sections determined from seismic refraction studies (*73*). In the model, extension also gives rise to exposure of gabbros (brown) and mantle rocks (green) (i) along a detachment-controlled flank, (ii) along the summit of the flexurally uplifted footwall block (the inside corner high), and (iii) in klippe distributed along the detachment surface (compare with MARK area exposures, Fig. 2A). Gabbros and serpentinites are also exposed at less prominent segment boundaries. If a segment boundary persists in time, outcrops of these rock types will be distributed on the ridge flanks approximately normal to the spreading axis or oblique to it if the segment boundary migrates along the ridge. In all cases, exhumation of lower crustal rocks results from footwall uplift along low-angle detachment faults that have accommodated a large amount of extension.

The highly extended region in the foreground of the model (Fig. 7) connects along axis to another asymmetric half-graben that has the opposite sense of polarity. They connect through an arcuate, oblique ridge (a doubly plunging antiform) in the axial depression (yellow) that is created by the overlap of oppositely facing detachment faults and lies at the morphologically defined center of a segment. The high marks the region where extensional strain is transferred from one major detachment fault to another with opposite dip and is one of a diverse class of transfer or accommodation zones like those known from continental extensional terranes (*58, 79, 80*). Border faults with arcuate shapes together with their associated transfer zones give rise to a structurally controlled axial morphology with an hourglass shape (*25*). The next closest segment includes a neovolcanic ridge (red) at its deepest end and is offset from the nearest segment at a discontinuity formed by overlap of two half-grabens; the elevated structure between is a more complex type of transfer zone (compare with the discontinuity at 29°23′N on the MAR, Fig. 2C). Transfer zones are indicated by the broad arrows in Fig. 7.

The elevated structures in the center of the morphologically defined segments and those found between axial depressions at segment boundaries are considered to be different expressions of the same tectonic process—the transfer of extensional strain between two adjacent half-grabens. Thus a single segment actually comprises two interconnected but independent structural units.

Ridge segments will evolve by cycles of magmatism and mechanical extension, each segment experiencing a history independent of others. The deep, detachment-controlled half-grabens mark regions where extension has evolved to the greatest extent and hence where the crust should be thinnest. Earthquakes on the MAR have recently been shown (*33*) to be deepest beneath the deepest parts of the spreading segment at 26°N. Such a distribution is consistent with deep penetration of detachment faults at segments boundaries. Furthermore, the pattern of crustal thickness variations derived from analysis of the axial gravity field (*55*) (Fig. 2D) shows that the crust is thinnest regionally at deep segment boundaries. The inferred Moho variations form an asymmetrical pattern, more like a sawtooth than a sinusoid, and we suggest that the gross pattern of the crustal structure is produced by overlapping crustal lozenges bound by detachments that result from the structural segmentation integral to the extension (Fig. 9).

The injection of an igneous body to form a neovolcanic ridge terminates an extensional cycle. Neovolcanic ridges are commonly located in the deepest parts of ridge segments (*25, 38*); we infer these to be regions of crustal thinning. A renewed cycle of mechanical extension begins as the igneous body is cooling and solidifying. Normal faults developed in the early stages of a new extensional cycle will be closely spaced, high-angle structures, and roughly symmetric grabens may form. As extension continues and the total strain increases, the grabens deepen and become increasingly asymmetric, and motion is taken up along low-angle detachment faults as in highly extended continental terranes (*81, 82*).

Finally, although we attribute the basic three-dimensional structure of slow ridges —their segmentation—to processes intrinsic to mechanical extension of the lithosphere and not to the passive response to magmatic processes, focusing of mantle flow and melt migration also has an important role in shaping the ridge at slow-spreading centers. Focused mantle upwelling will impart a three-dimensional pattern of temperature variations on the crust that will influence the crustal rheology by affecting the depth to the brittle-ductile transition. This in turn will influence the style and pattern of deformation such that large-scale brittle deformation is favored away from the warmer centers of upwelling. However, as evidence from continental rifts shows, the development of structural segmentation in extensional systems does not require thermally perturbed rheologies.

Thus we conclude that when spreading rates drop to less than about 35 mm/yr, the structure and segmentation of spreading ridges are primarily the expression of mechanical processes of extension. Segmentation scaling results from the geometry of large-scale detachment systems that accommodate amagmatic extension. These mechanical phenomena may be modulated by the three-dimensional thermal structure of the ridge, which is the manifestation of regional-scale lithospheric flow patterns and magma migration that construct the crust, but at these slow rates, the observed structures appear to result primarily from processes that deform the crust.

REFERENCES AND NOTES

1. K. C. Macdonald and P. J. Fox, *Earth and Planet. Sci. Lett.* **88**, 119 (1988).
2. R. M. Haymon *et al.*, *ibid.* **104**, 513 (1991).
3. J. A. Madsen, D. W. Forsyth, R. S. Detrick, *J. Geophys. Res.* **89**, 9997 (1984).
4. K. C. Macdonald, J.-C. Sempere, P. J. Fox, *ibid.*, p. 6049.
5. R. S. Detrick *et al.*, *Nature* **326**, 35 (1987).
6. J. Collier and M. Sinha, *ibid.* **346**, 646 (1990).
7. R. S. Detrick *et al.*, *Eos* **72**, 506 (1991).
8. S. C. Solomon, P. Y. Huang, L. Meinke, *Nature* **334**, 58 (1988).
9. B. C. Heezen, *Sci. Am.* **203**, 91 (1960).
10. N. H. Sleep, *J. Geophys. Res.* **80**, 4037 (1975).
11. J. R. Brown and J. A. Karson, *Mar. Geophys. Res.* **10**, 109 (1988).
12. G. M. Purdy and R. S. Detrick, *J. Geophys. Res.* **91**, 3739 (1986).
13. R. S. Detrick, J. C. Mutter, P. Buhl, I. I. Kim, *Nature* **347**, 61 (1990).
14. L. S. L. Kong, R. S. Detrick, P. J. Fox, L. A. Mayer, W. B. F. Ryan, *Mar. Geophys. Res.* **10**, 59 (1988).
15. P. Lonsdale, *J. Geophys. Res.* **88**, 9393 (1983).
16. ______, *Geol. Soc. Am. Bull.* **96**, 313 (1985).
17. K. C. Macdonald, D. S. Sheirer, S. M. Carbotte, *Science* **253**, 986 (1991).
18. C. H. Langmuir, J. F. Bender, R. Batiza, *Nature* **322**, 422 (1986).
19. Multichannel seismic (MCS) reflection profiling uses surface seismic sources and receivers and yields acoustic images of those simple boundaries or layers in the crust that have sufficient contrast with their surroundings (reflection coefficient) to cause a detectable level of seismic energy to be reflected back to the surface. The juxtaposition of different igneous rock types resulting from original magmatic layering or subsequent tectonism can produce detectable reflections, as can the locally anomalous properties of fault rocks or intrusions. Images are usually displayed in two-way reflection time (the scale at the right of Figs. 3, 4, and 5). The recovery of an image of a crustal boundary or layer depends on a combination of the energy level and bandwidth of the signal impinging on the boundary and the nature of the buried interfaces. Because seismic energy is attenuated with passage into the Earth, weak boundaries are typically imaged only at shallow levels of the crust, whereas only strong boundaries can be imaged at very deep levels. The field experiment only produces recordings of the Earth's acoustic response from which the image must be constructed by computer-based signal processing. Processing schemes vary widely and strongly affect the image quality [see (*20*)]. The images, except for Fig. 3 (top) and Fig. 5 (top), have been velocity-filtered and migrated with frequency-wavenumber techniques following stacking, bandpass filtering, and correction for geometric spreading.
20. Ö. Yilmaz, *Seismic Data Processing*, vol. 2 of *Investigations in Geophysics*, S. M. Doherty, Ed. (Society of Exploration Geophysicists, Tulsa, OK, 1987).
21. J. McCarthy *et al.*, *Geol. Soc. Am. Bull.* **100**, 1423 (1988).
22. R. S. White *et al.*, *Geology* **18**, 462 (1990).
23. E. Morris *et al.*, in preparation.
24. E. Banda, C. R. Ranero, J. J. Danobeitia, A. Rivero, *Geol. Soc. Am. Bull.*, in press.
25. J.-C. Sempéré, G. M. Purdy, H. Schouten, *Nature* **344**, 427 (1990).
26. G. M. Purdy *et al.*, *Mar. Geophys. Res.* **12**, 247 (1991).
27. ARCYANA, *Science* **190**, 108 (1975).
28. L. P. Zonenshain *et al.*, *Tectonophysics* **159**, 1 (1989).
29. C. Mevel *et al.*, *ibid.* **190**, 31 (1991).
30. D. R. Toomey *et al.*, *J. Geophys. Res.* **90**, 5443 (1985).
31. D. R. Toomey, S. C. Solomon, G. M. Purdy, *ibid.* **93**, 9093 (1988).
32. L. S. L. Kong, S. C. Solomon, G. M. Purdy, *ibid.* **97**, 1659 (1992).
33. J. Lin and E. A. Bergman, *Eos* **71**, 1572 (1990).
34. J.-M. Auzende *et al.*, *Nature* **337**, 726 (1989).
35. J. A. Karson and H. J. B. Dick, *Mar. Geophys. Res.* **6**, 51 (1983).
36. E. Bonatti, *Earth Planet. Sci. Lett.* **37**, 369 (1975).
37. P. J. Fox and J. B. Stroup, in *The Oceanic Lithosphere*, C. Emiliani, Ed. (Wiley, New York, 1981), pp. 119–218.
38. J. A. Karson *et al.*, *Nature* **328**, 681 (1987).
39. T. Juteau, E. Berger, M. Cannat, *Proc. Ocean Drilling Prog.* **106/109**, 27 (1990).
40. T. Juteau, M. Cannat, Y. Lagabrielle, *ibid.*, p. 303.
41. D. E. Kelly and J. R. Delaney, *Earth Planet. Sci. Lett.* **83**, 53 (1987).
42. M. Salisbury and N. Christensen, *ibid.*, p. 805.
43. J. A. Karson, *ibid.* **87**, 961 (1982).
44. P. Spudich and J. Orcutt, *Rev. Geophys. Space Phys.* **18**, 627 (1980).
45. K. Becker *et al.*, *Rev. Geophys.* **27**, 79 (1989).
46. H. J. B. Dick, G. Thompson, W. B. Bryan, *Eos* **62**, 406 (1981).
47. J. A. Karson, in *Oceanic Crustal Analogues*, J. Malpas, E. M. Moorse, A. Panayiotou, C. Xenopontos, Eds. (Geological Survey Department, Nicosia, Cyprus, 1990), pp. 547–555.
48. H. J. B. Dick *et al.*, *Proc. Ocean Drilling Prog.* **118**, 359 (1991).
49. G. T. Norrell and G. D. Harper, *Geology* **16**, 827 (1988).
50. J. F. Casey, *Eos* **68**, 1509 (1987).
51. Y. Dilek, E. M. Moores, M. Delaloye, J. A. Karson, in *Ophilite Genesis and Evolution of the Oceanic Lithosphere*, Tj. Peters *et al.*, Eds. (Kluwer, Dordrecht, 1991), pp. 485–500.
52. R. J. Varga, *J. Struct. Geol.* **13**, 517 (1991).
53. N. J. Schultz, R. S. Detrick, S. P. Miller, *Mar. Geophys. Res.* **10**, 41 (1988).
54. B. Y. Kuo and D. W. Forsyth, *ibid.*, p. 205.
55. J. Lin, G. M. Purdy, H. Schouten, J.-C. Sempere, C. Zervas, *Nature* **344**, 627 (1990).
56. W. Bosworth, *ibid.* **316**, 625 (1985).
57. B. R. Rosendahl *et al.*, in *Sedimentation in African Rifts*, L. E. Frostick *et al.*, Eds. (*Spec. Publ. 25*, Geological Society of London, London, 1986), pp. 29–43.
58. G. S. Lister, M. A. Etheridge, P. A. Symonds, *Geology* **14**, 246 (1986).
59. P.-H. Larsen, *J. Struct. Geol.* **10**, 3 (1988).
60. C. K. Morley, *Tectonics* **7**, 785 (1988).
61. J. R. Cochran and F. Martinez, *Eos* **70**, 465 (1989).
62. C. J. Ebinger, *Geol. Soc. Am. Bull.* **101**, 885 (1989).
63. J. A. Karson and P. C. Curtis, *J. Afr. Earth Sci.* **8**, 431 (1989).
64. B. Taylor *et al.*, *J. Geophys. Res.* **96**, 16113 (1991).
65. P. L. Stoffa, P. Buhl, T. J. Herron, T. K. Kan, W. J. Ludwig, *Mar. Geol.* **35**, 83 (1980).
66. Strictly, the Moho is defined as the interface or transition zone across which seismic velocities increase to greater than 8 km/s and is usually taken to lie at the top of the mantle. The location of the Moho therefore cannot be obtained directly from seismic reflection images, which do not resolve velocity structure sufficiently to define this transition. However, there are numerous examples where a strong basal reflector such as those in Fig. 3 has been recorded in regions where refraction measurements have established the depth of the transition, and these typically show that the reflector and the top of a layer with velocity in excess of 8 km/s approximately coincide. The term "reflection Moho" has come to describe a roughly horizontal reflector, or group of reflectors, in seismic images that occurs at the reflection time expected for the Moho based on seismic refraction measurements.
67. G. A. Barth and J. C. Mutter, *Eos* **72**, 490 (1991).
68. ______, J. A. Madsen, *Geology* **19**, 994 (1991).
69. J. H. Hopper, J. C. MMuller, R. L. Larson, C. Z. Mutter, the Northwest Australia Study Group, *ibid.*, in press.
70. J. A. Collins, G. M. Purdy, T. M. Brocher, *J. Geophys. Res.* **94**, 9283 (1989).
71. C. Z. Mutter, *Joint Oceanogr. Inst. U.S. Sci Adv. Comm. Newsl.* **5**, 4 (1992).
72. B. R. Rosendahl and H Groschel-Becker, *Eos* **72**, 428 (1991).
73. T. A. Minshull *et al.*, *J. Geophys. Res.* **96**, 9955 (1991).
74. "Flow line" is used to describe survey lines run perpendicular to the direction of seafloor spreading and hence in the direction that newly accreted lithosphere flows away from the spreading center. "Isochron line" refers to a line oriented parallel to the spreading axis at which the crust was formed and hence on lithosphere of constant age.
75. Layer structures can be estimated from these waveforms by defining a layer as two simple reflectors, one at the top and the other at the base. The reflection coefficients and reflector spacing are estimated by iteratively comparing the observed waveforms with that resulting from the convolution of the seismic source (derived from the seafloor return appropriately scaled for geometric spreading losses) with the trial two-point reflection series. Comparison is made by a least-squares optimization in which the final model is taken to be the one which minimizes the root mean square residual misfit between calculated and observed waveforms The frequency and phase response of a thin layer also depend critically on the layer thickness and velocity so the frequency spectrum of the observed waveforms can be used as an independent means of determining these parameters. The calculation presented in Fig. 6B was performed by E. E. Vera
76. S. J. Reynolds and G. S. Lister, *Geology* **18**, 216 (1990).
77. M. Ellis and G. King, *Science* **254**, 839 (1991).
78. H. J. B. Dick *et al.*, *Proc. Ocean Drilling Prog.* **118**, 439 (1991).
79. A. D. Gibbs, *Geol. Soc. London* **141**, 609 (1984).
80. C. K. Morley *et al.*, *Am. Assoc. Petrol. Geol. Bull.* **74**, 1234 (1990).
81. B. Wernicke, *Nature* **291**, 645 (1981).
82. G. S. Lister and G. A. Davis, *J Struct. Geol.* **11**, 65 (1989).
83. T. J. Dunkleman *et al.*, *Geology* **16**, 258 (1988).

84. This article represents the outgrowth of research conducted under a large number of individual grants over the past 10 years. Particularly important were grants from the Office of Naval Research (N00014-90-1043 and N0014-87-K-0074), the NSF's Division of Earth Sciences (EAR89-16351), and numerous grants from the Division of Ocean Sciences. We thank the two reviewers whose comments were very useful in identifying weaknesses in the original manuscript. J.C.M. also wishes to thank P. Buhl, J. Alsop, and J. B. Diebold, who provided advice on the analysis and preparation of reflection profiles, and E. E. Vera for analysis of waveform data Lamont-Doherty Geological Observatory contribution 4957.